Activated layered magnetism from bulk TiN

Chiung-Yuan Lin[1,*] Szu-Wen Yang,[1] Keng-Liang Ou,[2,3,4,5] and Barbara A. Jones[6,†]
[1]*Institute of Electronics, National Chiao Tung University, Hsinchu 300, Taiwan*
[2]*Department of Dentistry, Taipei Medical University Hospital, Taipei 110, Taiwan*
[3]*Department of Dentistry, Taipei Medical University-Shuang Ho Hospital, New Taipei City 235, Taiwan*
[4]*3D Global Biotech Inc., New Taipei City 221, Taiwan*
[5]*Department of Dentistry, Cathay General Hospital, Taipei 106, Taiwan*
[6]*IBM Research-Almaden, San Jose, California 95120–6099, USA*

(Received 14 November 2018; revised manuscript received 8 October 2019; published 24 December 2019)

The unexpected properties of a uniaxially expanded TiN bulk arising from increasing the layer spacing from equilibrium are explored using a first-principles approach. We reveal an unusual nonmagnetic-magnetic transition from a TiN bulk to its monolayer. We also investigate the electronic and magnetic structures of a few TiN atomic layers. We find that the bilayer and trilayer, like the TiN bulk, are nonmagnetic poor metals. On the other hand, the monolayer TiN is found to carry a magnetic moment on its Ti atoms, and likely be a semiconductor. The unpaired electron giving rise to magnetism on Ti is primarily in the orbital perpendicular to the layers, and we find it is freed to give rise to magnetism when the layers are slightly separated. We find two different antiferromagnetic states possible on the monolayer, as well as one ferromagnetic, with one of the antiferromagnetic being the lowest energy. The exchange couplings between Ti atoms in such a monolayer are calculated to be antiferromagnetic for both the nearest-neighbor and next-nearest-neighbor sites. We also analyze the binding nature of both the monolayer and bilayer TiN by examining the predominant binding orbitals.

DOI: 10.1103/PhysRevMaterials.3.124412

I. INTRODUCTION

Transition-metal nitrides have extraordinary material properties: high melting temperature [1,2], high hardness [1,2], high Curie temperature [3]. They are mostly electrical conductors, and some of their thin films even exhibit superconductivity [3]. As a result they are extensively studied by scientists. Among them titanium nitride (TiN) draws especially great attention. Its high hardness [1,2] and corrosion resistance [2] make it one of the best wear-resistant coatings of cutting and threading tools. It can also serve as conductive barrier layers in semiconductor devices for its good conductivity [2] and high diffusion barrier [4–6]. Other applications of TiN include coating costume jewelry with its metallic gold color and transparent thin films of selective wavelengths. Besides the variety of coating applications, its microscopic magnetism is also of potential considerable interest. Bulk TiN has no magnetism, not even microscopic antiferromagnetism [7]. On the other hand, a Ti atom carries a magnetic moment as a free atom and as an adatom on the surface [8–10]. This insight leads one to expect that a few atomic layers of TiN may exhibit magnetism, and such magnetism could be turned on/off by varying the layer spacing. These interesting properties would have a wide range of applications, such as highly sensitive magnetic sensors and actuators [11,12]. The atomic-scale structures can also potentially serve as biomedical magnetic coatings, e.g., on the acupuncture needle tip to increase its magnetic stimulation in the acupuncture points.

Atomically thin materials can turn into novel electronic structures. A single atomic layer of certain two-dimensional (2D) materials is substantially different from their van-der-Waals-stacked bulk: the mobility of graphene vs graphite [13,14], and the direct-bandgap transition metal dichalcogenides [15–17] vs their indirect-bandgap bulk [18,19]. The band gaps of conventional semiconductor thin films increase due to quantum confinement as the thickness shrinks [20,21]. Metallic ultrathin films exhibit unexpected growth behaviors when the film thickness is comparable to the Fermi wavelength [22]. In addition to electronic structure and transport properties, it is also demonstrated that atomic ultrathin layers may possess substantially different structural, chemical, and optical properties [23–25]. In another view, magnetism can be induced by bulk doping with magnetic dopants [26–28]. Likewise, a 2D material gains magnetic moments that are induced by point defects [29–32] or nanoribbon edges [33,34]. In addition to the line edges of 2D ribbons, a recent study demonstrates layer-dependent magnetic ordering from a bulk material CrI_3 down to its single atomic layer [35]. Likewise, even though for the material of interest of this study, TiN, no magnetism is found either for its pure bulk or when being implanted with foreign atoms [36,37], we expect, based on analogy to the effects of dimensionality in the nanoribbon examples earlier in this paragraph, that its few atomic layers (with its surfaces considered as planes of "vacancies" and/or "defects") are very likely to be magnetic. Past studies of atomic TiN layers have not yet revealed magnetism, either experimentally [38] or computationally [39,40].

*genelin@mail.nctu.edu.tw
†bajones@us.ibm.com

We are thus motivated to study nanolayers of TiN, to see under which conditions magnetism arises in this material. In this work, we calculate using density functional theory (DFT) a TiN monolayer that is formed within TiN bulk by inserting Ar atoms into the interstitials above and below. To further understand the fundamental properties we calculate one to several layers of TiN, as a simplified model system, and explore the transition from one monolayer of TiN to bulk properties. We start by calculating the electronic and magnetic structures of one, two, and three atomic layers of TiN. The magnetic properties include the magnetic moments, ferro- and antiferromagnetism, the magnetic couplings between Ti atoms, and the spin-resolved partial density of states (PDOS). The spin-resolved PDOS is further analyzed to determine from which particular orbital the magnetism originates. From that we can find the binding nature between atoms to obtain deeper insights into the electronic properties of these layered structures. Experimentally we would envision these few-layer systems as semi-free-standing unbuckled layers with, for example, van der Waals coupling to the substrate. Moreover, a nonmagnetic bulk and a possibly magnetic single layer for TiN imply that we may expand the lattice only along one axis to lift apart the bulk layers, and expect a magnetic-nonmagnetic transition as the bulk is expanded. We expand our study of the magnetism vs the number of atomic layers to the magnetism of a uniaxially expanded TiN bulk. Finally, we present our concluding discussion.

II. MATERIALS AND METHODS

TiN bulk crystallizes in the rocksalt structure, with a lattice constant we calculate to be 4.26 Å, in good agreement with the experimental value 4.24 Å [41]. We then construct its atomic monolayer, bilayer, and trilayer. Experiments have realized that TiN favors the growth of (001) and (111) oriented grains [42], and we have performed phonon calculations showing that the TiN(111) monolayer is unstable (see the Supplemental Material [43]). Therefore, all the above three modeled atomic ultrathin layers are chosen in the (001) direction, modeled as periodic slabs separated by vacuum of at least 20 Å. The lattice constants of one, two, and three atomic layers of TiN are taken to be the same as the bulk instead of their stress-free values (see the Supplemental Material [43] for explanations). In addition to the stand-alone monolayer mentioned above, we construct two additional monolayer structures, in order to more closely model possible experimental realizations of the layer expansion [44]. In both cases we use Ar as an artificial spacer, Ar chosen both for its convenient size and for its nonreactive nature. One structure is a monolayer of TiN sandwiched in bulk by Ar above and below, and the other is a surface monolayer separated from bulk by a layer of Ar. In both cases, we find that the Ar atoms are absorbed most stably at the Ti site of the bulk surface (details and the structural stability in Supplemental Material [43] "Ar atoms inserted into the TiN bulk resulting in TiN monolayer model systems"). The periodic superlattice structure contains five layers of TiN alternating with the Ar-TiN-Ar sandwich. The Ar-TiN top layer structure consists of a five-layer TiN slab, the Ar-TiN top layer, and above that a vacuum of at least 20 Å.

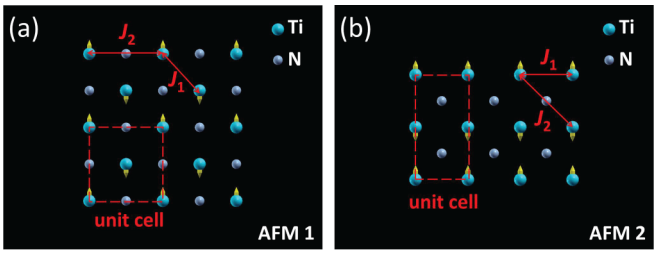

FIG. 1. Schematic diagrams showing antiferromagnetic spin configurations in a TiN monolayer. (a) Antiferromagnetic phase 1 (AFM1): opposite spins form two square sublattices in a checkerboard pattern. (b) Antiferromagnetic phase 2 (AFM2): opposite spins form alternating stripes. For both figures, the red dashed border lines specify the unit cells, and the yellow arrows indicate the spin directions. The exchange couplings J_1 and J_2 are associated with the Ti atoms as indicated.

In this study, we perform first-principles calculations within the framework of density functional theory (DFT), in the all-electron full-potential-linearized augmented-plane-wave (FLAPW) basis [45], with the exchange-correlation potential taken under the Perdew-Burke-Ernzerhof (PBE) generalized gradient approximation [46]. An additional onsite Coulomb repulsion U is added to the Ti $3d$ orbital (to be called PBE+U throughout this paper) basis, where the U values are calculated using the constraint-PBE method in the FLAPW [47]. The interlayer spacings of the bilayer and trilayer are further relaxed until all the forces between atoms reduce below 2mRy/bohr. For the Ar-inserted structures, the structure relaxations are instead performed in the projector-augmented wave (PAW) basis [48–50] with van der Waals force included [51]. We also examine the stability of the TiN monolayer, bilayer, and the Ar-inserted structures by calculating their phonon dispersions [52], also from first principles in the PAW basis. The electronic calculations of all above four TiN structures are used to further calculate their valence charges and spins by Bader analysis [53].

III. RESULTS

A. Magnetic phases

To understand the magnetic phases of the TiN monolayer, we calculate the exchange couplings between Ti atoms. The Heisenberg Hamiltonian $H = J\mathbf{S_1} \cdot \mathbf{S_2}$ provides the simplest estimation of those couplings, where the values of J is extracted from the energy differences between the ferromagnetic (FM) and antiferromagnetic (AFM) systems. We need to consider two antiferromagnetic phases in the FM-AFM energy difference in order to calculate the dominating J's that couple two nearest-neighbor and next-nearest-neighbor Ti atoms, namely J_1 and J_2 respectively (see Fig. 1). After carefully counting the couplings that occur in the unit cell of each antiferromagnetic phase, we relate J_1 and J_2 to the DFT-calculated transition energies between FM and AFM as follows:

$$\Delta E_1 = E_{\mathrm{FM}} - E_{\mathrm{AFM1}} = 8J_1|S|^2, \tag{1}$$

$$\Delta E_2 = E_{\mathrm{FM}} - E_{\mathrm{AFM2}} = 4J_1|S|^2 + 8J_2|S|^2, \tag{2}$$

TABLE I. The calculated magnetic moments of TiN bulk, monolayer, bilayer, and trilayer. The unit of magnetic moment is number of electrons. U is the coulomb repulsion applied to the Ti $3d$ orbital.

TiN Structure	U (eV)	Magnetic moment	
		Ti	N
Bulk	4.0	0.00	0.00
Monolayer (AFM1)	7.7	1.11	0.00
Bilayer	7.2	0.00	0.00
Trilayer	7.2	0.00	0.00

where S is the magnitude of spin, E_{FM} and E_{AFM} are the total energies of FM and AFM phases calculated by DFT, respectively.

The magnetic monolayer exhibits rich magnetic phases by different alignments of its atomic spins. There is a FM phase. Two AFM phases are also found, AFM1 and AFM2. The former consists of opposite atomic spins between nearest-neighbor Ti sites [Fig. 1(a)], while the latter has alternating spin orientations of (110) atomic-spin stripes [Fig. 1(b)]. We also explore the strength of the spin couplings as follows. The exchange couplings between nearest-neighbor and next-nearest-neighbor Ti atoms have been extracted to be $J_1 = 8.68$ meV and $J_2 = 2.54$ meV, both being antiferromagnetic. Notice that the nearest-neighbor coupling is roughly four times that of the next-nearest neighbor one, as expected. The energy differences between different magnetic phases provide an estimate of temperatures of magnetic phase transitions. In fact, the monolayer has its AFM1 phase 3.6 meV lower in energy than AFM2 (equivalent to a temperature ~40 K) per unit cell, and these two AFM phases are 17.4 meV (equivalent to a temperature of ~200 K) and 13.8 meV lower than the FM phase, respectively. Although the two antiferromagnetic phases are not too far apart in energy, clearly the AFM1 phase is the ground state, especially compared to the FM state.

B. Comparison of electronic and magnetic properties

We compare the electronic and magnetic properties of the TiN bulk, monolayer, bilayer, and trilayer. Using the constraint-PBE method [47], the U values of the above three structures are calculated to be 4.0, 7.7, 7.2, and 7.2 eV, respectively. By employing these U values, we calculate the magnetic moments and densities of states, as shown in Table I and Fig. 2. The bilayer and trilayer TiN contain no magnetic moment, like the bulk, and therefore we expect that TiN(001) thin films are nonmagnetic for two and more atomic layers. However, interestingly, in a surface-induced magnetism effect, the monolayer always carries a magnetic moment of 1.1 on its Ti atoms in its three different magnetic phases, and we conclude the Ti has $S = 1/2$ on a TiN monolayer. We further confirm this effect in structures of a surface monolayer separated from bulk by a layer of Ar, as well as a monolayer of TiN sandwiched in bulk by Ar above and below (see the Supplemental Material [43] "Ar atoms inserted into the TiN bulk resulting in TiN monolayer model systems"). In all three

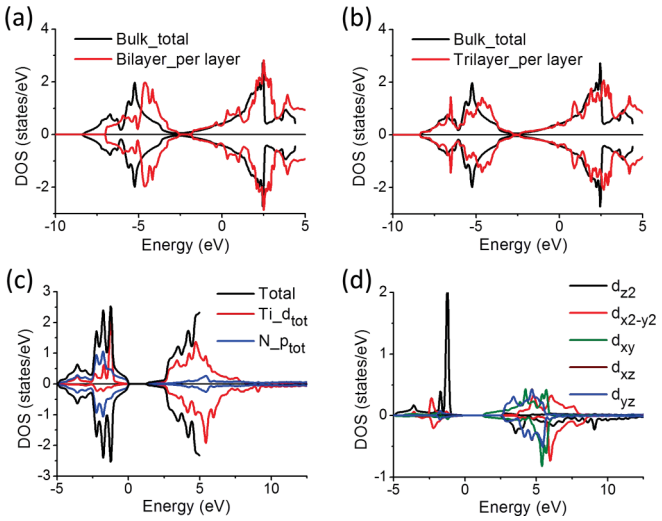

FIG. 2. The densities of states of TiN structures. (a) The total DOS of TiN bulk and the DOS per layer of the bilayer structures. (b) The total DOS of TiN bulk and the DOS averaged per layer of the trilayer structures. (c) For the AFM monolayer, the total density of states of the d electrons of the spin-up Ti, the p electrons of N, and the total electrons in the unit cell, including interstitial contributions. (Values of the total above 5 eV have been removed because the interstitial contributions are large and are not part of the current discussion.) (d) The Ti $3d$ PDOS of TiN monolayer structure, showing the unpaired electron in $3d_{z^2}$. For all four figures, positive (negative) refers to spin-up (spin-down).

cases, we find a separated monolayer displays an induced magnetism.

By comparing Ti $3d$ PDOS, band structures, and magnetic moments with and without spin-orbit coupling, we find the spin-orbit coupling to be negligible on the above-calculated electronic structures and magnetism (see the Supplemental Material [43] "The negligible spin-orbit coupling in a monolayer"). We first compare the DOS of the nonmagnetic bilayer and trilayer in Figs. 2(a) and 2(b) as referenced from the bulk, and find that the bilayer and trilayer systems not only both exhibit nonmagnetism but also have very similar density of states in their electronic structures. The electrical property of a TiN bulk is experimentally well known to be a poor metal [54]. To qualitatively determine the electrical properties of the bilayer and trilayer, we combine Boltzmann transport theory and DFT-calculated electronic structure to find the conductivity divided by the relaxation time σ/τ, whose square root is formally the thermodynamic root-mean square of the Fermi velocity times the fundamental charge (see details in Ref. [55]). We obtain σ/τ as 1.27×10^{21}, 1.50×10^{20}, and $2.11 \times 10^{20}\ \Omega^{-1}\,\mathrm{m}^{-1}\,\mathrm{s}^{-1}$ for the bulk, bilayer, and trilayer, respectively. Given the fact that surface scattering effects in the bilayer and trilayer will result in relaxation times shorter than the bulk, consequently bilayer and trilayer should have lower conductivity. We therefore expect that TiN(001) thin films beyond two atomic layers are also poor metals.

We can explain the origin of the magnetism of the monolayer in the following way. The monolayer has an abrupt unpaired spin-up DOS peak near $1 \sim 2$ eV below the Fermi level as shown in Fig. 2(d). This is also apparent in the DOS

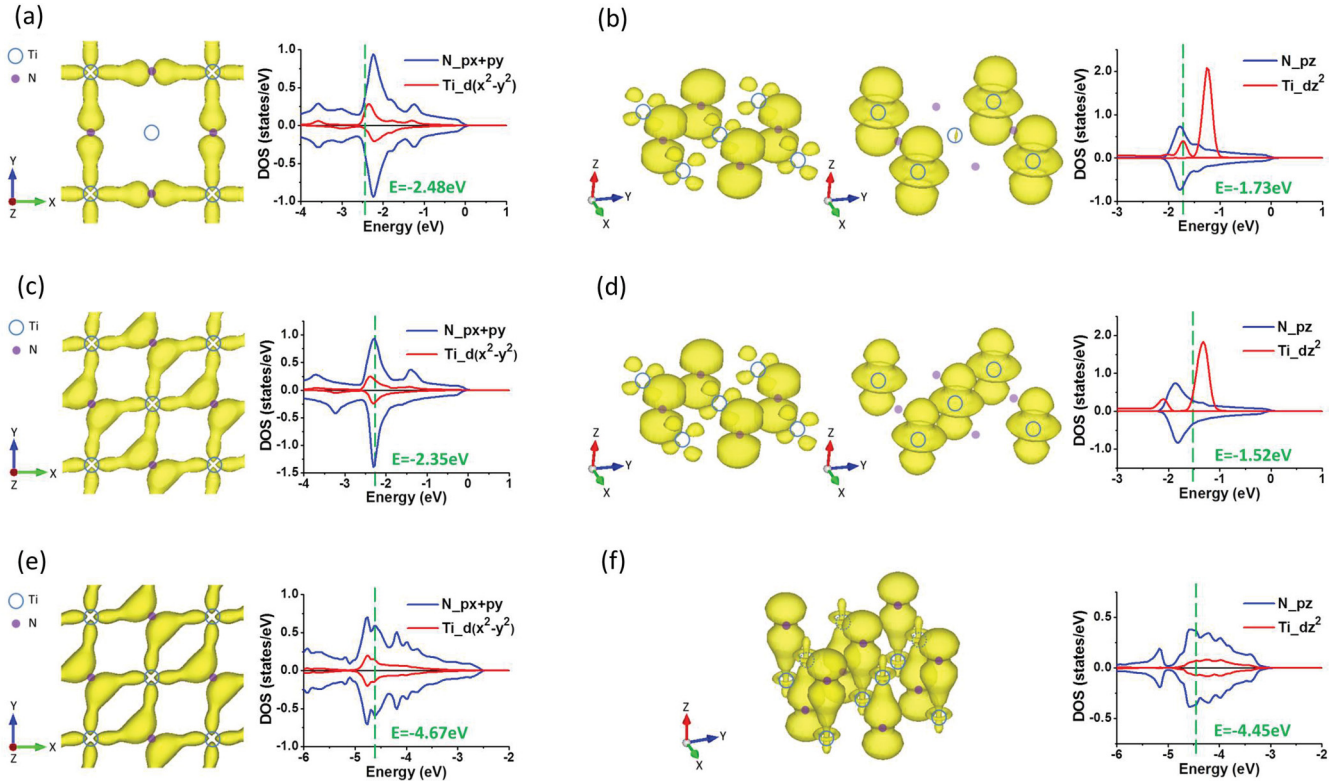

FIG. 3. Isosurface plots of the Ti-N binding orbitals for TiN monolayer and bilayer. Three plotted systems include two of the TiN-monolayer magnetic phases, AFM1 in (a) and (b) and FM in (c) and (d), and the nonmagnetic bilayer in (e) and (f). The vertical green dashed lines in all PDOS plots indicate the energy of their associated orbitals. (a) One representative in-plane binding orbital; the PDOS shows it has a N p_x, p_y + Ti $d_{x^2-y^2}$ binding nature. (b) Two representative out-of-plane dangling orbitals; the PDOS shows the two degenerate orbitals have orbital natures of N p_z + Ti ($d_{xz} + d_{yz}$) and Ti d_{z^2}, respectively. (c) One representative in-plane binding orbital; the PDOS shows a N ($p_x + p_y$) + Ti $d_{x^2-y^2}$ binding nature. (d) Two representative out-of-plane, degenerate dangling orbitals; the PDOS shows they have orbital natures of N p_z + Ti ($d_{xz} + d_{yz}$) and Ti d_{z^2}, respectively. (e) One representative in-plane binding orbital; the PDOS shows a N($p_x + p_y$) + Ti $d_{x^2-y^2}$ binding nature. (f) One representative out-of-plane binding orbital; the PDOS shows a N p_z + Ti d_{z^2} binding nature. [Note that in (a) and (b) there are two interpenetrating square lattices of opposite spin. We show up spin only here. The other sublattice would appear identical.]

of Ti in Fig. 2(c), which additionally shows that N does not carry a spin. The Ti PDOS of all five 3d orbitals are plotted in Fig. 2(d), further showing that the unpaired electron basically occupies the 3d_{z^2} orbital, which is calculated to contribute a magnetic moment of almost one unpaired electron. We will interpret this result in more detail in the next subsection.

We calculated the electronic structure of the monolayer using PBE+U. However, based on the established methodology to obtain the best estimation of the band gap for materials such as TiO_2, which involves not only addition of a U_d to the d orbitals of the transition metal but also another U_p to the p orbitals of the first-row reactive nonmetal, we add a U term to the p orbital of N in the monolayer. We see that the bandgap decreases from 1.25 to 1.11 eV as U_p is increased from 0 to 6 eV. Based on this analysis, we expect the bandgap of TiN monolayers lies between 1.11 and 1.25 eV. This bandgap would make TiN monolayers semiconductive.

In summary, we show that the TiN(001) monolayer is an antiferromagnetic semiconductor, the unpaired electron residing primarily in the Ti 3d_{z^2} orbital. However, in a sudden transition, any other numbers of layers become nonmagnetic poor conductors. (In the Supplemental Material [43] are further comparisons of magnetism with Ti and N binding on material surfaces.) In the rest of this paper we explore in detail the magnetic phases of the monolayer, how the magnetic/nonmagnetic transition arises, and, how it can be controlled.

C. Binding orbitals

In order to understand the binding natures of the mono- and bilayer TiN, we search for the particular orbitals that dominate the bonds, and determine their orbital symmetries by both plotting and quantitative decomposition. We find that an AFM1 TiN monolayer has the peaks of the N $p_x + p_y$ and Ti $d_{x^2-y^2}$ spin-up PDOS align at many energies, as shown in Fig. 3(a). We focus on one Kohn-Sham orbital that exhibits almost pure coupling in the plane. The plotted orbital in Fig. 3(a) shows strong in-plane binding hybridized by N p_x and Ti $d_{x^2-y^2}$. Similar analyses find two degenerate representative out-of-plane orbitals, plotted in Fig. 3(b). One state has N p_z and Ti $d_{xz} + d_{yz}$ with N dominant. The other state has Ti d_{z^2} with Ti dominant, with no N present.

In the next row of this figure, we examine the binding of the ferromagnetic phase, because it will be instructive when we come to the bilayer. The greatest binding forms between

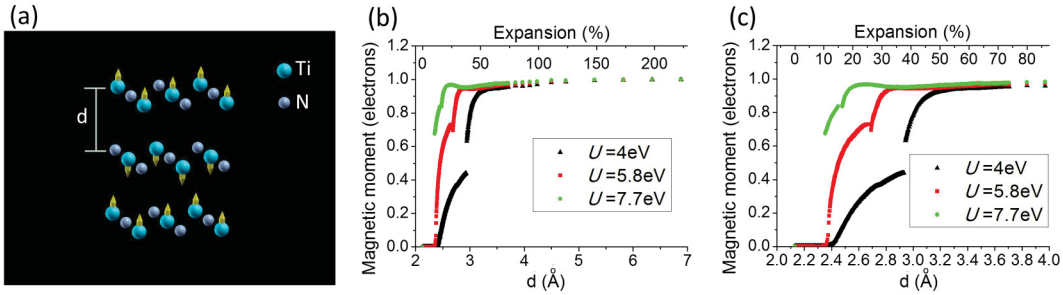

FIG. 4. Predicted magnetic transition due to a uniaxial expansion on TiN bulk. (a) Schematic plot of a uniaxially expanded TiN bulk, where d is the layer spacing. The yellow arrows indicate the direction of the Ti spins. (b) and (c) The calculated magnetic moments per unit cell per layer, as functions of d with $U = 4, 5.8, 7.7$ eV, respectively. The upper axis shows the respective percentage of expansion in d. In (c), we have a closer look at the transition in (b).

N $p_x + p_y$ and Ti $d_{x^2-y^2}$ modes [Fig. 3(c)]. Notice that the bonds in plane differ from those in AFM1. In Fig. 3(d), we plot the orbital of monolayer FM out of plane. Notice the strong similarity to the orbitals out of plane for AFM1 [Fig. 3(b)]. The difference in the surface symmetry in the two figures is solely due to difference of AFM and FM magnetic configurations (explained further in the figure caption).

Now we come to the bilayer, where the magnetism approaches zero. Here the nature of the interlayer binding is of greatest interest. Fig. 3(f) shows a broad copeak of the N p_z and Ti d_{z^2} PDOS as well as the representative wave function, indicating very strong interlayer hybridization between N p_z and Ti d_{z^2}. We also plot the corresponding quantities for the in-plane binding for a bilayer, and this is shown in Fig. 3(e). Notice the interesting correspondence of these images to those of the monolayer ferromagnetic along-the-plane case. In contrast, the out-of-plane orbitals for the bilayer look very different from the monolayer case, because of the strong hybridization between layers in the bilayer case. The binding for thicker layers all look similar to those of the bilayer.

D. Magnetic transition from the nonmagnetic bulk to the magnetic monolayer

One way to consider controlling the magnetic transition between the TiN bulk and monolayer is to slowly lift apart the bulk layers originally stacked at the equilibrium lattice spacing until each bulk layer becomes far apart enough to reasonably mimic one monolayer. The details of the magnetic moments at the intermediate layer spacings bring us closer to such a magnetic-nonmagnetic transition.

In principle, one should use a varying U to the above lattice-expansion calculations, with the U value calculated by the constraint-PBE method on the fly. However, besides being computationally expensive, brute-force calculations of the U values with varying layer spacing often encounter convergence problems at the intermediate layer spacings of rapidly varying magnetic moments. As an alternative, we calculate the uniaxially expanded bulk at three fixed U values: the bulk (4 eV), the monolayer (7.7 eV), and their average (5.8 eV).

We calculate the expanded TiN bulk in the atomic-spin configuration in Fig. 4(a), with FM moments within each layer and AFM coupling between layers (see also an additional configuration in the Supplemental Material [43] "Magnetic transition from the nonmagnetic bulk to the magnetic monolayer: AFM within each layer"). The calculated magnetic moments are plotted in Fig. 4(b), as functions of the layer spacing along the expanded direction, with all three U values. In the cases of all three U values we show [expanded in Fig. 4(c)] that the TiN bulk basically remains nonmagnetic with a uniaxial layer spacing below 2.4 Å, and undergoes a nonmagnetic-magnetic transition when the spacing is stretched between 2.4 and 2.7 Å. As the layer spacing keeps being stretched beyond 3.2 Å, the magnetic moments approach the value of a monolayer. Hence, we have here captured the essence of the nonmagnetic-magnetic transition.

IV. DISCUSSION

By calculating the electronic structure of ultrathin TiN atomic layers, we reveal the exotic electronic and magnetic transitions by varying the number of layers: A single-layer TiN exhibits physical properties totally different from its multilayers. The latter are nonmagnetic, poor conductors, similar to the bulk, while the former is a magnetic semiconductor with two nearly degenerate AFM phases. The TiN monolayer has one $3d_{z^2}$ unpaired electron per Ti atom, and it may undergo an AFM-FM transition around the temperature of dry ice. Moreover, our further investigations into a bilayer indicate that the above $3d_{z^2}$ magnetic orbital becomes hybridized with the N p_z of the other layer, and consequently its orbital magnetism gets quenched for two layers and more.

The unexpected surface-induced magnetism of a TiN monolayer, contrary to its nonmagnetic bulk, inspires us to further look into the details. We did this in two ways. Our calculations show that inserting Ar into a TiN bulk or on the surface to create a TiN surface layer will produce magnetism on the TiN monolayer. In a second way, we examine a uniaxially expanded TiN bulk. Such a bulk undergoes, as observed from first-principles calculations, a nonmagnetic-magnetic transition by increasing the layer spacing only along the c axis. This transition is found to have an onset at a 13% expansion, and saturates into monolayer magnetism at 27%.

In fact, our calculations suggest that experimentalists can practically fabricate a magnetic TiN monolayer within a TiN bulk or on the surface by alternatingly depositing molecules and TiN on a substrate or in general by separating layers molecularly. Revealing the unusual magnetic transition induced by uniaxial expansion in a computational study provides innovative directions to further engineer the magnetism

of TiN and develop applications of great impact in biomedical coating of tunable magnetism, magnetoresistive sensors, and magnetostrictive ultrathin-film actuators.

ACKNOWLEDGMENTS

We thank R. Pushpa and S. Gangopadhyay for their stimulating discussions. C.-Y.L. and S.-W.Y. are partially funded by Taiwan Ministry of Science and Technology Grants No. MOST 104-2112-M-009-005, No. MOST 104-2119-M-009-008, No. MOST 105-2119-M-009-009, No. MOST 107-2633-E-009-003, No. MOST 108-2633-E-009-001, and No. MOST 108-3017-F-009-003, and by the "Center for Semiconductor Technology Research" of National Chiao Tung University from The Featured Areas Research Center Program within the framework of the Higher Education Sprout Project of Taiwan Ministry of Education and also acknowledge the facility support from the Taiwan National Center for High-Performance Computing. K.-L.O. and S.-W.Y. acknowledge financial support from Taiwan Ministry of Health and Welfare Grant No. MOHW103-TDU-N-211-133001. The work of B.A.J. was performed in part at the Aspen Center for Physics, which is supported by National Science Foundation Grant No. PHY-1607611.

[1] D. R. Lide (ed.), *CRC Handbook of Chemistry and Physics* (Internet Version 2005, CRC, Boca Raton, FL, 2005).
[2] C. Wang, Y. Dai, H. Gao, X. Ruan, J. Wang, and B. Sun, Solid State Commun. **150**, 1370 (2010).
[3] H. Allmaier, L. Chioncel, and E. Arrigoni, Phys. Rev. B **79**, 235126 (2009).
[4] J. S. Chen and K.-Y. Lu, Thin Solid Films **396**, 204 (2001).
[5] M. Moriyama, T. Kawazoe, M. Tanaka, and M. Murakami, Thin Solid Films **416**, 136 (2002).
[6] M. Y. Kwak, D. H. Shin, T. W. Kang, and K. N. Kim, Thin Solid Films **339**, 290 (1999).
[7] M. G. Brik and C.-G. Ma, Comput. Mater. Sci. **51**, 380 (2012).
[8] A. F. Otte, M. Ternes, K. V. Bergmann, S. Loth, H. Brune, C. P. Lutz, C. F. Hirjibehedin, and A. J. Heinrich, Nat. Phys. **4**, 847 (2008).
[9] K. Yang, Y. Bae, W. Paul, F. D. Natterer, P. Willke, J. L. Lado, A. Ferrón, T. Choi, J. Fernández-Rossier, A. J. Heinrich, and C. P. Lutz, Phys. Rev. Lett. **119**, 227206 (2017).
[10] Y. Xie and P. R. C. Kent, Phys. Rev. B **87**, 235441 (2013).
[11] M. Pasquale, Sens. Actuators A **106**, 142 (2003).
[12] S. A. Wilson, R. P. J. Jourdain, Q. Zhang, R. A. Dorey, C. R. Bowen, M. Willander, Q. U. Wahab, M. Willander, S. M. Al-hilli, O. Nur, E. Quandt, C. Johansson, E. Pagounis, M. Kohl, J. Matovic, B. Samel, W. van der Wijngaart, E. W. H. Jager, D. Carlsson, Z. Djinovic, M. Wegener, C. Moldovan, R. Iosub, E. Abad, M. Wendlandt, C. Rusu, and K. Persson, Mater. Sci. Eng. R. Rep. **56**, 1 (2007).
[13] A. K. Geim and K. S. Novoselov, Nat. Mater. **6**, 183 (2007).
[14] A. K. Geim, Science **324**, 1530 (2009).
[15] K. F. Mak, C. Lee, J. Hone, J. Shan, and T. F. Heinz, Phys. Rev. Lett. **105**, 136805 (2010).
[16] W. Zhao, Z. Ghorannevis, L. Chu, M. Toh, C. Kloc, P.-H. Tan, and G. Eda, ACS Nano **7**, 791 (2013).
[17] Y. Zhang, T.-R. Chang, B. Zhou, Y.-T. Cui, H. Yan, Z. Liu, F. Schmitt, J. Lee, R. Moore, Y. Chen, H. Lin, H.-T. Jeng, S.-K. Mo, Z. Hussain, A. Bansil, and Z.-X. Shen, Nat. Nanotechnol. **9**, 111 (2014).
[18] H. Jiang, J. Phys. Chem. C **116**, 7664 (2012).
[19] T. Böker, R. Severin, A. Müler, C. Janowitz, R. Manzke, D. Voß, P. Krüger, A. Mazur, and J. Pollmann, Phys. Rev. B **64**, 235305 (2001).
[20] Z. H. Lu and D. Grozea, Appl. Phys. Lett. **80**, 255 (2002).
[21] E. G. Barbagiovanni, D. J. Lockwood, P. J. Simpson, and L. V. Goncharova, J. Appl. Phys. **111**, 034307 (2012).
[22] M. M. Özer, C.-Z. Wang, Z. Zhang, and H. H. Weitering, J. Low Temp. Phys. **157**, 221 (2009).
[23] V. O. Özçelik, K. Gong, and C. E. White, Nano Lett. **18**, 1786 (2018).
[24] L. Sun, X. Yan, J. Zheng, H. Yu, Z. Lu, S.-P. Gao, L. Liu, X. Pan, D. Wang, Z. Wang, P. Wang, and L. Jiao, Nano Lett. **18**, 3435 (2018).
[25] S. Gupta, S. N. Shirodkar, A. Kutana, and B I. Yakobson, ACS Nano **12**, 10880 (2018).
[26] A. Berlie, J. W. White, M. Henderson, and S. Cottrell, Phys. Rev. Mater. **1**, 054405 (2017).
[27] D. Chiba, F. Matsukura, and H. Ohno, J. Phys. D **39**, R215 (2006).
[28] T. Dietl, Nat. Mater. **9**, 965 (2010).
[29] O.V. Yazyev and L. Helm, Phys. Rev. B **75**, 125408 (2007).
[30] J. Yun, Y. Zhang, M. Xu, K. Wang, and Z. Zhang, Mater. Chem. Phys. **182**, 439 (2016).
[31] J. Yang, D. Kim, J. Hong, and X. Qian, Surf. Sci. **604**, 1603 (2010).
[32] D. S. Fartab and A. A. Kordbacheh, Superlattice. Microstruct. **118**, 185 (2018).
[33] A. R. Botello-Méndez, F. López-Urías, M. Terrones, and H. Terrones, Nanotechnology **20**, 325703 (2009).
[34] F. López-Urías, A. L. Elías, N. Perea-López, H. R. Gutiérrez, M. Terrones, and H. Terrones, 2D Mater. **2**, 015002 (2015).
[35] B. Huang, G. Clark, E. Navarro-Moratalla, D. R. Klein, R. Cheng, K. L. Seyler, D. Zhong, E. Schmidgall, M. A. McGuire, D. H. Cobden, W. Yao, D. Xiao, P. Jarillo-Herrero, and X. Xu, Nature (London) **546**, 270 (2017).
[36] M. Popović, M. Novaković, M. Mitrić, K. Zhang, and N. Bibić, Int. J. Refract. Met. Hard Mater. **48**, 318 (2015).
[37] M. Popović, M. Novaković, M. Mitrić, K. Zhang, Z. Rakočević, and N. Bibić, Mater. Res. Bull. **91**, 36 (2017).
[38] K. Khlifi and A. B. C. Larbi, J. Adhes. Sci. Technol. **28**, 85 (2014).
[39] R.-Q. Zhang, C.-E. Kim, B. Delley, C. Stampfl, and A. Soon, Phys. Chem. Chem. Phys. **14**, 2462 (2012).
[40] L. Zhou, Z. Zhuo, L. Kou, A. Du, and S. Tretiak, Nano Lett. **17**, 4466 (2017).
[41] J. M. Schneider, A. Voevodin, C. Rebholz, A. Matthews, J. H. C. Hogg, D. B. Lewis, and M. Ives, Surf. Coat. Technol. **74–75**, 312 (1995).

[42] D. Gall, S. Kodambaka, M. A. Wall, I. Petrov, and J. E. Greene, J. Appl. Phys. **93**, 9086 (2003), and the references therein.

[43] See Supplemental Material at http://link.aps.org/supplemental/10.1103/PhysRevMaterials.3.124412 for TiN monolayer and bilayer, Ar atoms inserted into the TiN bulk resulting in TiN monolayer model systems, the negligible spin-orbit coupling in a monolayer, magnetism of Ti in different surroundings, and magnetic transition from the nonmagnetic bulk to the magnetic monolayer: AFM within each layer.

[44] J. Nathan Hohmanat Molecular Foundry, Lawrence Berkeley National Lab, and other experimental colleagues at other institutions (private communication).

[45] P. Blaha, K. Schwarz, G. K. H. Madsen, D. Kvasnicka, and J. Luitz, *WIEN2k, An Augmented Plane Wave + Local Orbitals Program for Calculating Crystal Properties* (Karlheinz Schwarz, Techn. Universität Wien, Austria, 2001).

[46] J. P. Perdew, K. Burke, and M. Ernzerhof, Phys. Rev. Lett. **77**, 3865 (1996).

[47] G. K. H. Madsen and P. Novák, Europhys. Lett. **69**, 777 (2005).

[48] G. Kresse and J. Furthmüller, Phys. Rev. B **54**, 11169 (1996); Comput. Mater. Sci. **6**, 15 (1996).

[49] P. E. Blöchl, Phys. Rev. B **50**, 17953 (1994).

[50] G. Kresse and D. Joubert, Phys. Rev. B **59**, 1758 (1999).

[51] S. Grimme, J. Antony, S. Ehrlich, and H. Krieg, J. Chem. Phys. **132**, 154104 (2010).

[52] A. Togo and I. Tanaka, Scr. Mater. **108**, 1 (2015).

[53] R. F. W. Bader, Acc. Chem. Res. **18**, 9 (1985).

[54] B. O. Johansson, J.-E. Sundgren, J. E. Greene, A. Rockett, and S. A. Barnett, J. Vac. Sci. Technol. A **3**, 303 (1985).

[55] G. K. H. Madsen and D. J. Singh, Comput. Phys. Commun. **175**, 67 (2006).